Research Article

Computational Identification and Structural Analysis of Deleterious Functional SNPS in CHN1 Gene Causing Duane Retraction Syndrome

Jincy Anna Jomy, Rao Sethumadhavan*

*Bioinformatics Division, School of Bio Sciences and Technology, VIT University, Vellore, Tamil Nadu, India.

***Corresponding author's E-mail:** rsethumadhavan@vit.ac.in

Accepted on: 18-11-2014; **Finalized on:** 31-12-2014.

ABSTRACT

Here we have evaluated the Single Nucleotide Polymorphisms (SNPs) that can alter the expression and the function in CHN1 gene through computational methods. To explore possible relationships between genetic mutations and phenotypic variation, different computational methods like Sorting Intolerant from Tolerant (SIFT, an evolutionary-based approach), Polymorphism Phenotyping (PolyPhen, a structure-based approach) and I-Mutant 3.0 (support vector machine based tool) are discussed. There were 7 missense mutations; in this we observed 5 variants that were deleterious and damaging respectively. We got 6 non-synonymous SNPs (nsSNPs) (85.71%) to be deleterious by SIFT, I- Mutant 3.0 and PolyPhen-2. Then cation-π interactions in protein structures are identified and analyzed the roles played by Arg, Lys interactions with π (Phe, Tyr or Trp) residues and their role in the structural stability. Then docking analysis between 1MH1 and the native and mutant modeled structures have done. Subsequently, modeling of these 5 variants was performed to understand the change in their conformation with respect to the native CHN1 by computing their root mean square deviation (RMSD). Those 4 missense mutation were due to loss of stability in their mutant structures of CHN1. This was confirmed by computing their total energies using GROMOS 96 force field and these mutations were cross validated with computational programs.

Keywords: Missense mutation, CHN1, RMSD, Total energy, RAC1, π- interactions

INTRODUCTION

Duane's retraction syndrome (DRS) is a congenital eye movement disorder characterized by adduction deficiency, abduction limitation, globe retraction, and palpebral fissure narrowing on attempted adduction[1]. DRS is the frequent cause of strabismus in children and may result in amblyopia-related visual loss. Some of the data suggest that DRS may result from abnormal development or absence of the abducens nerve (cranial nerve VI)[2]. As the six muscles help in eye movement, the improper movement of these eye muscles causes Duane syndrome i.e. the sixth cranial nerve that controls the lateral rectus muscle (the muscle that rotates the eye out towards the ear) does not develop properly[3].

The problem occurs not only with the eye muscles, but also with nerves, that transmits the electrical impulses to the muscle. The eye deviates upward and downward is a main symptom of DRS. Sometimes the head position of patients often maintain a head posture or head turn to keep the eyes straight and in some cases the eye appear to be smaller than the other one. Duane retraction syndrome-2 (DURS2; 604356) is caused by mutation in the CHN1 gene (118423) on chromosome 2q31[2]. CHN1 (chimerin 1) mutations can hyperactivate α2-chimaerin and result in aberrant cranial motor neuron development[4]. CHN1 gene disrupts the normal development of these nerves and the extraocular muscles needed for side-to-side eye movement. Abnormal function of these muscles leads to restricted eye movement and related problems with vision[1,6,7,8].

Mutational analysis suggests that CHN1 interacts with RAC1. Ras-related C3 botulinum toxin substrate 1 (Rac1) is a protein found in human cells which encodes RAC1 gene. The protein N-chimaerin is responsible for the cause of DRS, which activates CHN1 gene.

Seven mutations in the CHN1 gene have been identified in families with isolated Duane retraction syndrome[9]. In this study we are screening these mutations using computational tools and the commonly affected deleterious mutants are taken. Then we will be finding out some of features of a protein, how they interact and their structure stability. In addition to that we are finding out the cation-π interactions to find out the stability. In proteins, C–H....π interactions occur between the C atom of main- or side-chain amino acid residue and the aromatic side chains of phenylalanine (F), tyrosine (Y), tryptophan (W) and histidine (H). Here we are trying to focus on protein properties such as secondary structure involvement, solvent accessibility, interaction range, stabilization centers and conservation score[10]. The substrate, RAC1, was then docked with both the native protein and mutants to determine the binding effect and the nature of the flexibility in the binding pockets, which explained the decreased binding efficiency of these missense mutations[11].

MATERIALS AND METHODS

Datasets

The SNPs and their related protein structures were obtained from the Swissprot and PDB database for our computational analysis.[12-14]

SIFT, Sequence Homology based Method for Functional Consequence of nsSNP

The SIFT predicts whether submitted nsSNP affected the protein function based on sequence homology and amino acid properties. SIFT is a sequence homology-based tool which predicts the variants as neutral or deleterious using normalised probability score. The degree of conservation of a particular position in a protein was determined through this tool. It is a multistep procedure which searches for similar sequences, chooses closely related sequences that may share similar function, obtains the multiple alignment of these chosen sequences, and calculates normalized probabilities for all possible substitutions at each position from the alignment.

If the tolerance index score is less than 0.05, then it is predicted to be deleterious and which is greater than 0.05 is considered to be neutral[15-16].

PolyPhen, Structure Homology based Method for Functional change in Point Mutant

PolyPhen 2.0 is a structural homology based tool. It calculates position-specific independent counts (PSIC) scores for each of the two variants and then computes the PSIC scores difference between them. It analyzes the damaged point mutations at the structural level is considered to be very important to understand the functional activity of the concerned protein.

The higher the PSIC score difference, the higher the functional impact a particular amino acid substitution would be likely to have[17].

I-Mutant 3.0, Support Vector Machine Tool for Protein Stability

I-Mutant 3.0 is a suite of Support Vector Machine (SVM) based predictors incorporated in a unique web server which gives the opportunity to predict protein stability changes upon single-site mutations based on Gibbs free energy. The output files show the predicted free energy change value or sign ($\Delta\Delta G$), which was calculated from the unfolding Gibbs free energy value of the mutated protein minus the unfolding Gibbs free energy value of the native protein (kcal mol^{-1}).

Positive $\Delta\Delta G$ values meant that the mutated protein has higher stability and negative values indicate lower stability[19-20].

Modeling Single Amino Acid Polymorphism (SAAP) Location on Protein Structure to compute the RMSD

Structure analysis was performed to evaluate the structural deviation between native proteins and mutant proteins by means of root mean square deviation (RMSD). We used the web resource Protein Data Bank and the single amino acid polymorphism database (SAAPdb) to identify the 3D structure of CHN1 (PDB ID: 3CXL)[21]. We also confirmed the mutation position and the mutation residue in PDB ID 3CXL. The mutation was performed *in silico* using the SWISSPDB viewer, and NOMAD-Ref server performed the energy minimization for 3D structures[22]. As the server uses Gromacs as the default force field for energy minimization, based on the methods of steepest descent, conjugate gradient, and limited-memory Broyden-Fletcher-Goldfarb-Shanno (L-BFGS)[23-24] methods, we used conjugate gradient method to minimize the energy of the 3D structure of CHN1. To optimize the 3D structure of CHN1, we used the ifold server for simulated annealing which efficiently samples the vast conformational space of biomolecules in both length and time scales.

Divergence of the mutant structure from the native structure could be caused by substitutions, deletions and insertions and the deviation between the two structures could alter the functional activity with respect to binding efficiency of the inhibitors, which was evaluated by their RMSD values[25-27].

Computation of Total Energy and Stabilizing Residues

Total energy indicates the stability between native and mutant modeled structures, and could be computed by the GROMOS96 force field that is embedded in the SWISSPDB viewer. Molecular mechanics or force field methods use classical type models to predict the energy of the molecule as a function of its conformation. It allows us to predict equilibrium geometries, transition states and relative energies between conformers or between different molecules. Performing energy minimization and simulated annealing removes steric clashes and to obtains the best stable conformation. Total energy was computed for native and mutants by GROMOS force field[28-29]. To identify the stabilizing residues for both the native and mutant structures represented a significant parameter for understanding their stability. We have used the server SRide to identify the stabilizing residues in the native and mutant protein models. Stabilizing residues were computed using parameters such as surrounding hydrophobicity, long-range order, stabilization center, and conservation score[30].

Computation of Cation–π Interactions Energy

Cation-π interactions in protein structures are identified and evaluated by using an energy-based criterion for selecting significant side chain pairs. These cation–π interactions are obtained using CaPTURE program. Cation-π interactions are found to be common among structures in the Protein Data Bank.

The total Cation–π interaction energy (Ecat–π) has been divided into electrostatic (Ees) and van der Waals energy (Evw) and was computed using the program CaPTURE, which had implemented a subset of OPLS force field[21] to calculate the energies[31-32].

The Ecat-π is the sum of these two energies, i.e., electrostatic and the van der Waals energy.

$$E_{cat-\pi} = E_{es} + E_{vdW}$$

Conservation Score Calculation

The conservation score of residues were calculated using Consurf server (http://consurf.tau.ac.il/). Conservation score is a useful parameter for the identification of conserved residues in a protein sequence[35-36].

Secondary Structure and Solvent Accessibility

We obtained the information about secondary structures and solvent accessibility of the proteins using the program DSSP. Solvent accessibility was divided into three classes: buried, partially exposed, and exposed indicating respectively the least, moderate, and high accessibility of the amino acid residues to the solvent. The structure and function of proteins is determined by two important intermediate factors. They are secondary structure preference and solvent accessibility patterns. In order to obtain the preference and pattern of each cation-π interaction-forming residue in glycoproteins, we conducted a systematic and careful analysis based on their location in different secondary structures and their solvent accessibility[37-38].

Calculating the Total number of Intra Molecular Interactions using PIC Server

To compute the intra-molecular and inter molecular interactions for native and mutants structures is done by Protein Interactions Calculator. PIC server accepts atomic coordinate set of a protein structure in the standard Protein Data Bank (PDB) format. Interactions within a protein structure and interactions between proteins in an assembly are essential considerations in understanding molecular basis of stability and functions of proteins and their complexes. There are several weak and strong interactions that render stability to a protein structure or an assembly. It computes various interactions such as interaction between a polar residues, disulphide bridges, hydrogen bond between main chain atoms, hydrogen bond between main chain and side chain atoms, hydrogen bond between two side chain atoms, interaction between oppositely charged amino acids (ionic interactions), aromatic- aromatic interactions, aromatic-sulphur interactions and cation-π interactions[39].

Analysing the Binding Affinity between CHN1 and RAC1

To find the binding affinity between CHN1 and Ras-related C3 botulinum toxin substrate 1 (Rac1), we used the protein-protein docking server, GRAMM-X which is based on GRAMM Fast Fourier Transformation methodology by employing smoothed potentials, refinement stage, and knowledge-based scoring[40]. Then, the docked protein complex is given to the DFIRE server as an input for calculating the binding free energy (ΔG) score. It used a new reference state called the distance-scaled, finite ideal-gas reference (DFIRE) state. It is a distance-dependent structure-derived potential developed so far and all employed a reference state that can be characterized as a residue (atom)-averaged state. In addition, the DFIRE-based all-atom potential provides the most accurate prediction of the stabilities of mutants based on knowledge-based all-atom potentials[41].

RESULTS AND DISCUSSION

Single Amino Acid Polymorphism Dataset from Swissprot

The CHN1 and a total of 7 variants namely L20FI, 126M, Y143H, A223V, G228S, P252Q and E313K were retrieved from Swissprot database (Table 1).

Table 1: List of Functionally Significant Mutants predicted to be by SIFT, I-Mutant 3.0 and PolyPhen-2

Variants	SIFT	PolyPhen	I-Mutant 3.0
L20F	**0**	**0.97**	**-0.89**
I126M	0.91	0.042	**-1.27**
Y143H	**0.01**	**0.998**	**-1.15**
A223V	**0.02**	**0.999**	0
G228S	**0**	**0.998**	**-1**
P252Q	**0**	**0.954**	**-1.18**
E313K	**0.01**	**0.983**	**-1.29**

Notes: Letters in bold indicate mutants predicted to be less stable, deleterious and damaging by I-Mutant 3.0, SIFT and PolyPhen-2 respectively.

Deleterious Single Point Mutants identified by the SIFT Program

The protein sequences of the 7 variants were submitted to SIFT to determine their tolerance indices. As the tolerance level increases, the functional influence of the amino acid substitution decreases and vice versa. Here the 6 variants were found to be deleterious with tolerance index scores of ≤0.05 (Table 1). Among these 6 variants, 3 variants showed a very high deleterious tolerance index score of 0.00. Two variants showed tolerance index score of 0.01 and one variant showed 0.02. Interestingly, all the deleterious variants identified by SIFT also were seen to be less stable by the Polyphen server.

Damaging Single Point Mutations identified by the PolyPhen Server

The protein sequence with mutational position and amino acid variants associated with the 7 single point mutants were submitted to the PolyPhen server. A PSIC score difference of 0.5 and above was considered to be damaging. Out of 7 variants, 6 were considered to be damaging by PolyPhen (Table 1). These variants exhibited a PSIC score difference from 0.95 to 0.99. The variants were found to be damaging by PolyPhen program were also deleterious by SIFT and also by Mutant 3.0 except A223V.

Identification of Functional variants by I-Mutant 3.0

Of the 7 variants, 6 were found to be less stable using the I-Mutant 3.0 server (Table 1). Among these 6 variants, 4 variant showed a ΔΔG value between <-1 and <-1.29 and

one variants showed a ΔΔG value >-0.89 as depicted in Table 1.

Rational Consideration of Detrimental Point Mutations

We have considered the 5 most potential detrimental point mutations (L20FI, Y143H, G228S, P252Q and E313K) for further course of investigations because they were commonly found to be less stable, deleterious and damaging by the I-Mutant3.0, SIFT and Poly Phen-2 servers respectively[19-21]. As we consider the statistical accuracy of these three programs, I-Mutant improves the quality of the prediction of the free energy change caused by single point protein mutations by adopting a hypothesis of thermodynamic reversibility of the existing experimental data. The accuracy of prediction for sequence and structure based values were 78% and 84% with correlation coefficient of 0.56 and 0.69, respectively[42]. SIFT correctly predicted 69% of the substitutions associated with the disease that affect protein function. PolyPhen-2 evaluates rare alleles at loci potentially involved in complex phenotypes, densely mapped regions identified by genome-wide association studies, and analyses natural selection from sequence data, where even mildly deleterious alleles must be treated as damaging. PolyPhen-2 was reported to achieve a rate of true positive predictions of 92%[42-44]. To obtain precise and accurate measures of the detrimental effect of our variants, comprehensive parameters of all these three programs could be more significant than individual tool parameters.

Hence, we further investigated these detrimental missense mutations by structural analysis. Figure 1 shows the list of functionally significant mutations with the commonly affected ones.

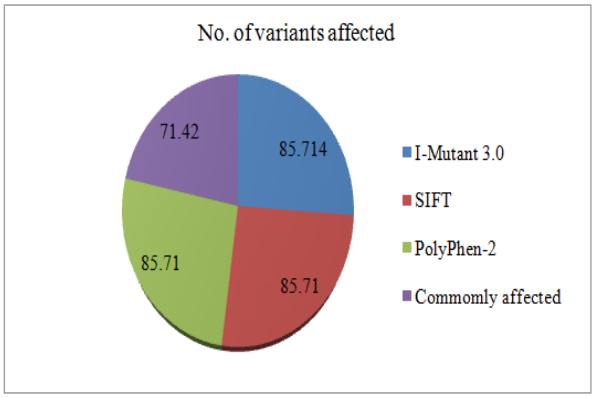

Figure 1: List of Functionally Significant Mutations

Computing the RMSD by Modeling of Mutant Structures

The available structure of CHN1 is PDB ID 3CXL. The mutational position and amino acid variants were mapped onto 3CXL native structure. Mutations at a specified position were performed *in silico* by SWISSPDB viewer independently to obtain a modeled structure. NOMAD-Ref server[22] and ifold server[25] performed the energy minimizations and stimulated annealing respectively, for both native structure and the 7 mutants modeled structures. To determine the deviation between the native structure and the mutants, we superimposed the native structures with all 7 mutant modeled structures and calculated the RMSD. The higher the RMSD value, the more deviation there is between the native and mutant structure, which in turn changes the binding efficiency with the substrate because of deviation in the 3D space of the binding residues of CHN1.

Table 2 shows the RMSD values for native structure with each mutant modeled structure. Table 2 shows that, one variant, L20F exhibited a high RMSD >2.00 Å and the other four variants exhibited an RMSD >1.00 Å.

Application of GROMOS 96 and SRIDE for Native Structure and Mutant Modeled Structures.

The total energy was calculated for both native and mutant structures. Table 2 shows that total energy of native structure was -13542.394 kcal mol^{-1}. Whereas the 2 mutant structures all had slightly higher total energies and 3 have lesser total energies compared with the native structure. Note that the higher the total energy, the lesser the stability and vice versa. We then used the SRide server to identify the stabilizing residues of both the native structure and the mutant modeled structures (Table 2). The native structure has only one stabilizing residue whereas on the other hand, 2 mutant structures have one stabilizing residue and the other 3 were showing no stabilizing residue was found because of less stringent threshold criteria. This indicates that 2 mutants L20F and E313K were less stable than the native structure. We further evaluated the effect of these detrimental missense mutations by performing binding analysis between CHN1 and RAC1 using docking studies.

Computing the Intra-Molecular Interactions in CHN1

We further validated the stability of protein structure by using the PIC server[39] to identify the number of intra-molecular interactions for both native and mutant structures (Table 3). Interactions within a protein structure and the interactions between proteins in an assembly were essential considerations in understanding molecular basis of stability and functions of proteins and their complexes. There were several weak and strong intra-molecular interactions that render stability to a protein structure. Therefore these intra-molecular interactions were computed by PIC server in order to further substantiate the stability of protein structure. Based on this analysis, we found that a total number of 1108 intra-molecular interactions were obtained in the native structure of CHN1. On the other hand, 5 mutant structures of CHN1 established the intra-molecular interactions between the range of 1166 to 1507 as shown in Table 3.

We further evaluated the effect of these 5 detrimental missense mutations by performing binding analysis between CHN1 and RAC1 through protein-protein docking studies in order to understand the functional activity of CHN1.

Table 2: RMSD, Total Energy and Stabilizing Residues for the Native Protein and Mutants.

Variants	RMSD	Total energy (Kj/mol)	No: of SR	Stabilizing residues
Native		-13542.4	1	CYS222
L20F	2.58Å	-24875.2	1	PRO294
Y143H	0.41Å	-12321	-	No Stabilizing Residue was found! You may specify less stringent threshold criteria.
G228S	0.41Å	-11222	-	No Stabilizing Residue was found! You may specify less stringent threshold criteria.
P252Q	0.51Å	-17909.8	-	No Stabilizing Residue was found! You may specify less stringent threshold criteria.
E313K	0.39Å	-9044.07	1	CYS178

Notes: RMSD- Root Mean Square Deviation; SR- Stabilizing residues; the common stabilizing residues are shown in bold

Table 3: Number of Intra-Molecular Interactions of the Native Protein and Mutants

Variants	Total	HI	MM	MS	SS	II	AA	AS	CI
3CXL	1108	338	489	126	97	28	18	7	5
L20F	1507	369	574	294	201	35	20	8	6
Y143H	1166	347	513	136	102	37	17	8	6
G228S	1169	352	510	135	105	35	18	8	6
P252Q	1184	353	523	139	102	37	18	6	6
E313K	1167	351	509	137	104	34	18	8	6

Notes: Total no of intramolecular interactions. HI- Hydrogen Interactions, MM- Main chain-Main chain interaction, MS- Main chain Side chain interaction, SS- Side chain side chain interactions, II- Ionic-Ionic interaction, AA- Aromatic-Aromatic interactions, AS- Aromatic-Sulphur interactions, CI- Cation-π interactions

Table 5: Secondary Structure

PDB ID	Cat-residue	2° str	ASA	π-residue	2° str	ASA	D_{seq}
Native_3CXL	R281	S	18	Y396	H	67	115
	K368	H	118	Y443	H	65	75

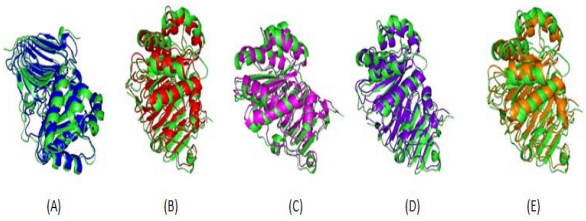

Figure 2: Superimposed Structure of the Native Protein (Green) with Mutant

(A) Superimposed structure of native CHN1 (green) with mutant L20F (blue) structure showing RMSD of 2.58Å (B) Superimposed structure of native CHN1 (green) with mutant Y143H (red) structure showing RMSD of 0.41Å (C) Superimposed structure of native CHN1 (green) with mutant G228S (magenta) structure showing RMSD of 0.41Å (D) Superimposed structure of native CHN1 (green) with mutant P252Q (violet) structure showing RMSD of 0.51Å. (E) Superimposed structure of native CHN1 (green) with mutant E313K (orange) structure showing RMSD of 0.39Å.

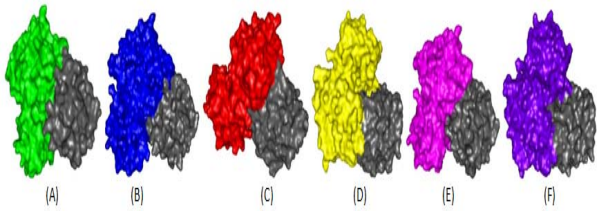

Figure 3: Docked Complexes of Native and Mutant CHN1 with RAC1

(A) Docked complex of Native CHN1 (green) and RAC1 (grey) having the Free energy of -1022.37, (B) Docked complex of L20F (blue) and RAC1 (grey) having the Free energy of -1053.73, (C) Docked complex of Y143H (red) and RAC1 (grey) having the Free energy of -1019.57, (D) Docked complex of G228S (yellow) and RAC1 (grey) having the Free energy of -1022.65, (E) Docked complex of P252Q (magenta) and RAC1 (grey) having the Free energy of -1022.79, (F) Docked complex of E313K (violet) and RAC1 (grey) having the Free energy of -1009.37.

Table 6: Average Cation-π Interaction Energy

PDB ID	R-F (-Kcal/mol)	R-Y (-Kcal/mol)	R-W (-Kcal/mol)	K-F (-Kcal/mol)	K-Y (-Kcal/mol)	K-W (-Kcal/mol)
3CXL	-	R281-Y396(-8.31)	-	-	K368-Y443(-2.76)	-
L20F	-	R281-Y396 (8.31)	-	-	K368-Y443 (-2.76)	-
Y143H	-	R281-Y396 (8.31)	-	-	K368-Y443 (-2.76)	-
G228S	-	R281-Y396 (8.31)	-	-	K368-Y443 (-2.76)	-
P252Q	-	R281-Y396 (8.31)	-	-	K368-Y443 (-2.76)	-
E313K	-	R281-Y396 (8.31)	-	-	K368-Y443 (-2.76)	-

Analyzing the Binding Efficiency for Native and Mutant

In order to find out the binding efficiency of native and mutant RAC1, we implemented molecular dynamics approach for rationalizing the functional activity of these 5 mutants. In this analysis, we performed 5 missense mutations (L20FI, Y143H, G228S, P252Q and E313K) in the chain A of the PDB IDs 3CXL and 1MH1 by swisspdb viewer independently and energy minimization was performed for the entire complex (both native and mutant complex) by GROMACS (Nomad-ref) followed by simulated annealing to get the optimized structures using a discrete molecular dynamics approach (ifold). We used Grammx to dock CHN1 native and mutant structures with RAC1 and furthermore; we used DFire, for finding the protein conformation free energy source for the docked complex retrieved from Grammx. We used this server for the missense mutation analysis with respect to finding the free energy source of both native and mutants of RAC1. In this analysis, we found that the binding free energy for RAC1 with native CHN1 protein was found to be -1022.37 kcal/mol, has a higher binding affinity compared to the mutants. This analysis portrays that native CHN1 exhibited higher binding affinity with RAC1. Hence, the lesser binding free energies may probably be due to loss of intermolecular non-covalent interactions. This analysis clearly portrayed that native complex had high intermolecular non covalent interactions than mutant complexes.

Energetically Significant Cation–π Interactions

Table 4: No of Intramolecular Interactions, Atomic Contact Energy and Free Energy for the Native protein and Mutants

Variants	Total no. of Intramolecular Interactions	Atomic Contact Energy (ACE)	Free Energy (Kcal/mol)
Native	1108	-103.10	-1022.37
L20F	1507	-470.2	-1053.73
Y143H	1166	-23.19	-1019.57
G228S	1169	-91.08	-1022.65
P252Q	1184	-2.88	-1022.79
E313K	1167	-175.06	-1009.37

Notes: R- Arginine, F- Phenylalanine, Y- Tyrosine, W- Tryptophan, K- Lysine

The Cation–π interaction energy of both native and mutant prion proteins was analysed. The two pairs of cation-π interactions (Arginine- Tryptophan and Arginine-Tryptophan) in native are -8.31 and -2.76 respectively (Table 4). On the other hand mutants show -8.31 and -2.76, which has almost similar energy which shows cation-π interactions. The results are shown in Figure 2.

Secondary Structure Preferences

The occurrence of weak interactions has been observed at the terminus of the secondary structural units, in particular α-helix and β-sheets[46,47]. These interactions play a definitive role in stabilizing the proteins. Here we have calculated the occurrence of cation-π forming residues in secondary structure. We found that the cation-π forms Strands (S) and Turns (T) which is shown in Table 5.

CONCLUSION

Of the 7 variants that were retrieved from Swissprot, 6 variants were found less stable by I-Mutant2.0, 6 variants were found to be deleterious by SIFT and 6 variants were considered damaging by PolyPhen. Five variants were selected as potentially detrimental point mutations because they were commonly found to be less stable, deleterious and damaging by the I-Mutant 3.0, SIFT and Poly-Phen-2.0 servers, respectively.

The structures of these 5 variants were modeled and the RMSD between the mutants and native structures ranged from 0.39Å to 2.58Å. Docking analysis between 1MH1 and the native and mutant modeled structures generated Free Energy scores between -1009.37 and -1053.73. Finally, we concluded that the lower binding affinity of 5 mutants (L20FI, Y143H, G228S, P252Q and E313K) with RAC1 compared with CHN1 in terms of their Free energy and RMSD scores identified them as deleterious mutations.

Thus the results indicate that our approach successfully allowed us to (1) consider computationally a suitable protocol for missense mutation (point mutation/single amino acid polymorphism) analysis before wet lab experimentation and (2) provided an optimal path for further clinical and experimental studies to characterize CHN1 mutants in depth.

REFERENCES

1. Miller NR, Kiel SM, Green WR, Clark AW, Unilateral Duane's retraction syndrome (Type 1), Archives of Ophthalmology, 100, 1982, 1468-1472.
2. Appukuttan B, Elizabeth G, Suh-Hang J, Diana F, Sandra O, Raman S, Ann VA, Joan B, Xiaoguang W, Reshma JP, Christiane MR, Mina C, Geralyn A, Kenneth W, Mark SB, Jeffrey MT, Michael JB, Timothy S, Localization of a gene for Duane retraction syndrome to chromosome 2q31, American journal of human genetics, 65, 1999, 1639–1646.
3. Mohsen Azarmina, Hossein Azarmina, The Six Syndromes of the Sixth Cranial Nerve, Journal of Ophthalmic & Vision Research, 8, 2013, 160–171.
4. Noriko Miyake, John Chilton, Maria Psatha, Long Cheng, Caroline Andrews, Wai-Man Chan, Krystal Law, Moira Crosier, Susan Lindsay, Michelle Cheung, James Allen, Nick J Gutowski, Sian Ellard, Elizabeth Young, Alessandro Iannaccone, Binoy Appukuttan, J. Timothy Stout, Stephen Christiansen, Maria Laura Ciccarelli, Alfonso Baldi, Mara Campioni, Juan C. Zenteno, Dominic Davenport, Laura E. Mariani, Mustafa Sahin, Sarah Guthrie, Elizabeth C. Engle, Human CHN1 mutations hyperactivate α2-chimaerin and cause Duane's retraction syndrome, Science, 321, 2008, 839-843.
5. Yip YL, Scheib H, Diemand AV, Gattiker A, Famiglietti LM, Gasteiger E, Bairoch A, The Swiss-Prot variant page and the

ModSNP database: a resource for sequence and structure information on human protein variants, Human Mutation, 23, 2004, 464–470.

6. Chung M, Stout JT, Borchert MS, Clinical diversity of hereditary Duane's retraction syndrome, Ophthalmology, 107, 2000, 500-503.
7. Evans JC, Frayling TM, Ellard S, Gutowski NJ, Confirmation of linkage of Duane's syndrome and refinement of the disease locus to an 8.8-cM interval on chromosome 2q31, Human genetics, 106, 2000, 636-638.
8. Miyake N, Chilton J, Psatha M, Cheng L, Andrews C, Chan WM, Law K, Crosier M, Lindsay S, Cheung M, Allen J, Gutowski NJ, Ellard S, Young E, Iannaccone A, Appukuttan B, Stout JT, Christiansen S, Ciccarelli ML, Baldi A, Campioni M, Zenteno JC, Davenport D, Mariani LE, Sahin M, Guthrie S, Engle EC, Human CHN1 mutations hyperactivate alpha2-chimaerin and cause Duane's retraction syndrome, Science, 321, 2008, 839-843.
9. Iftikhar Aslam Tayubi, Rao Sethumadhavan, Theoretical understanding of C–H....Π interactions and their distribution in immunoglobulin proteins-insilco geometrical approach, International Journal of Pharmacy and Pharmaceutical Sciences, 3, 2011, 212-218.
10. Rajasekaran R, Sethumadhavan R, In silico identification of significant detrimental missense mutations of EGFR and their effect with 4-anilinoquinazoline-based drugs, Applied Biochemistry and Biotechnology, 160, 2010, 1723–1733.
11. Sreevishnupriya K, Chandrasekaran P, Senthilkumar A, Sethumadhavan R, Shanthi V, Daisy P, Nisha J, Ramanathan K, Rajasekaran R, Computational analysis of deleterious missense mutations in aspartoacylase that cause Canavan's disease, Science China Life sciences, 55, 2012, 1190-1119.
12. Yip YL, Famiglietti M, Gos A, Duek PD, David FP, Gateau A, Bairoch A, Annotating single amino acid polymorphisms in the UniProt/Swiss-Prot knowledgebase, Human mutation, 29, 2008, 361-366.
13. Boeckmann B, Bairoch A, Apweiler R, Blatter MC, Estreicher A, Gasteiger E, Martin MJ, Michoud K, O'Donovan C, Phan I, Pilbout S, Schneider M, The SWISS-PROT protein knowledgebase and its supplement TrEMBL in 2003, Nucleic acids research, 31, 2003, 365-370.
14. Berman HM, Westbrook J, Feng Z, Gilliland G, Bhat TN, Weissig H, Shindyalov IN, Bourne PE, Nucleic Acids Research, 28, 2000, 235-242.
15. Ng PC, Henikoff S, SIFT: Predicting amino acid changes that affect protein function, Nucleic acid research, 31, 2003, 3812-3814.
16. Ng PC, Henikoff S, Predicting deleterious amino acid substitutions, Genome Research, 11, 2001, 863-874.
17. Ramensky V, Bork P, Sunyaev S, Human non-synonymous SNPs: server and survey, Nucleic acid research, 30, 2002, 3894-3900.
18. Capriotti E, Fariselli P, Casadio R, I-Mutant2.0: predicting stability changes upon mutation from the protein sequence or structure, Nucleic Acid Research, 33, 2005, 306-310.
19. Bava KA, Gromiha MM, Uedaira H, Kitajima K, Sarai A, ProTherm, version 4.0: thermodynamic database for proteins and mutants, Nucleic Acid Research, 32, 2004, 120-121.
20. Berman HM, Westbrook J, Feng Z, Gilliland G, Bhat TN, Weissig H, Shindyalov IN, Bourne PE, The Protein Data Bank, 28, 2000, 235-242.
21. Erik Lindahl, Cyril Azuara, Patrice Koehl, Marc Delarue, NOMAD-Ref: visualization, deformation and refinement of macromolecular structures based on all-atom normal mode analysis, 34, 2006, 52-56.
22. Delarue M and Dumas P, On the use of low-frequency normal modes to enforce collective movements in refining macromolecular structural models, Proceedings of the National Academy of Sciences of the United States of America, 101, 2004, 6957-6962.
23. Sharma S, Ding F, Nie H, Watson D, Unnithan A, Lopp J, Pozefsky D, Dokholyan NV, iFold: a platform for interactive folding simulations of proteins, Bioinformatics, 22, 2006, 2693.
24. Han JH, Kerrison N, Chothia C, Teichmann SA, Divergence of interdomain geometry in two-domain proteins, Structure, 14, 2006, 935-945.
25. Rajasekaran R, Sethumadhavan R, Exploring the cause of drug resistance by the detrimental missense mutations in KIT receptor: computational approach, Amino acids, 39, 2010, 651-660.
26. Varfolomeev SD, Uporov IV, Fedorov EV, Bioinformatics and molecular modeling in chemical enzymology. Active sites of hydrolases, Biochemistry, 67, 2002, 1099-1108.
27. Lukas D. Schuler, Xavier Daura, Wilfred F, Van Gunsteren, An Improved GROMOS96 Force Field for Aliphatic Hydrocarbons in the Condensed Phase, Journal of Computational Chemistry, 22, 2001, 1205.
28. Leach AR, Molecular Modeling: Principles and Applications. 2nd ed. Sussex: Pearson Education EMA, second edition, 2001.
29. Chou KC, Carlacci L, Simulated annealing approach to the study of protein structures, Protein engineering, 4, 1991, 661-667.
30. Magyar C, Gromiha MM, Pujadas G, Tusnády GE, Simon I, SRide: a server for identifying stabilizing residues in proteins, Nucleic Acid Research, 33, 2005, 303-305.
31. Gallivan JP, Dougherty DA, Cation-pi interactions in structural biology, Proceedings of the National Academy of Sciences of the United States of America, 17, 1999, 9459-9464.
32. Ramanathan K, Shanthi V, Rao Sethumadhavan, Contribution of cation-Π interaction and its effect on the structural stability of laccase enzymes-A computational study, International Journal of Pharma and Bio Sciences, 1, 2010, 1-15.
33. Glaser F, Pupko T, Paz I, Bell RE, Bechor-Shental D, Martz E, Ben-Tal N, ConSurf: identification of functional regions in proteins by surface-mapping of phylogenetic information, Bioinformatics, 19, 2003, 163-164.
34. Iftikhar Aslam Tayubi, Rao Sethumadhavan, Theoretical understanding of C–H....Π interactions and their distribution in immunoglobulin proteins-insilico

geometrical approach, International Journal of Pharmacy and Pharmaceutical Sciences, 3, 2011, 212-218.

35. Tayubi IA, Sethumadhavan R, Nature of cation-pi interactions and their role in structural stability of immunoglobulin proteins. Biochemistry, 75, 2010, 912-918.
36. Wolfgang Kabsch, Christian Sander, Dictionary of protein secondary structure: Pattern recognition of hydrogen-bonded and geometrical features, Biopolymers, 22, 1983, 2577-2637.
37. Tina KG, Bhadra R, Srinivasan N, PIC: Protein Interactions Calculator, Nucleic Acid Research, 35, 2007, 473-476.
38. Tovchigrechko A, Vakser IA, GRAMM-X public web server for protein-protein docking, Nucleic Acids Research, 34, 2006, 310-314.
39. Yuedong Y, Yaoqi Z, Ab initio folding of terminal segments with secondary structures reveals the fine difference between two closely related all-atom statistical energy functions, Protein science, 17, 2008, 1212-1219.
40. Emidio Capriotti, Piero Fariselli, Ivan Rossi, Rita Casadio, A three-state prediction of single point mutations on protein stability changes, 9, 2008, 1471-2105.
41. Kumar P, Henikoff S, Ng PC, Predicting the effects of coding non-synonymous variants on protein function using the SIFT algorithm, Nature protocols, 4, 2009, 1073-1081.
42. Adzhubei IA, Schmidt S, Peshkin L, Ramensky VE, Gerasimova A, Bork P, Kondrashov AS, Sunyaev SR, A method and server for predicting damaging missense mutations, Nature methods, 7, 2010, 248–249.
43. Fabiola GF, Krishnaswamy S, Nagarajan V, Pattabhi V, C-H...O hydrogen bonds in beta-sheets, Acta crystallographica, 53, 316-320.
44. Madan Babu M, Kumar Singh S, Balaram P, A C-H triple bond O hydrogen bond stabilized polypeptide chain reversal motif at the C terminus of helices in proteins, journal of molecular biology, 322, 2002, 871-880.

Source of Support: Nil, **Conflict of Interest:** None.